Korean J. Chem. Eng., 34(11), 2933-2943 (2017)
DOI: 10.1007/s11814-017-0194-y

pISSN: 0256-1115
eISSN: 1975-7220

Evaluating the ability of separation and adsorption of SO_2 by nano-CuO-Fe_2O_3/TiO_2 in high concentrations and moderate temperatures

Sina Esfandiarpour*, Mohammad Reza Ehsani*,†, Parisa Nazemi Ashani*, and Mohammad Hossein Enayati**

*Chemical Engineering Department, Isfahan University of Technology, Isfahan 84156-83111, Iran
**Material Engineering Department, Isfahan University of Technology, Isfahan 84156-83111, Iran
(*Received 30 January 2017 • accepted 8 July 2017*)

Abstract−Nano CuO-Fe_2O_3/TiO_2 adsorbents were made with different compositions of metal oxides using precipitation-desorption method. The adsorbents were applied for adsorption of SO_2 at high concentrations ranging from 10,000 to 30,000 ppm and temperatures between 523 and 627 K. Adsorption experiments were applied for adsorbents in a laboratory fixed bed adsorption column. The adsorption capacity was measured by calculating the area under the adsorption curve using the integral method. The results showed that temperature is the most affecting factor on the adsorption capacity. The highest adsorption capacity was obtained by using 17, 8 and 75 wt% of CuO, Fe_2O_3 and nano TiO_2, respectively. Characteristics of the best sorbent were determined by using Fe-SEM, XRD and nitrogen adsorption-desorption analyses.

Keywords: Removal of SO_2, Nano-adsorbent, Chemical Adsorption, Desulfurization, Metal Oxides

INTRODUCTION

SO_2 emissions are one of the major causes of smog and acid rain that may lead to health problems, such as sore throats, asthma and respiratory and lung diseases. Economic and environmental damage may include the demolition of forests, damage to monuments, and loss of genetic variation in species [1-4]. The global emissions of SO_2 can be attributed to natural and human activities. Human activities, which are the main sources of SO_2 emissions, include burning fossil fuels in power plants, boilers, furnaces, and other industrial operations [2,4,5].

Due to the pace of industrial growth throughout the world and the increased legislation related to the emissions of environmental pollutants, methods and strategies that can reduce SO_2 emissions into the atmosphere have attracted much attention from scientists and governments [6]. For example, the Claus process produces an output gas, called Claus tail gas, that contains acid gases, such as H_2S, SO_2, COS, and CS_2. These acid gases are absorbed by an amine-based process in the tail gas clean-up unit (TGCU) to satisfy the environmental limitations for atmospheric emissions [7-9].

The main disadvantages of removing acid gases using amines, as with other wet removal processes, are the excessive consumption of water, the pollution of the water through waste, the production of amine by-products, and the high cost of amines [10]. Due to these disadvantages and the problem of water shortages, there is a need for alternative methods to absorb acidic gases.

Methods that use dry solid sorbents, such as carbonaceous adsorbents, metal oxides, and silica-based mesoporous materials, have received the most attention as a possible solution to replace methods that consume significant amounts of water [2]. Studies have shown that the removal performance of carbonaceous adsorbents for SO_2 was improved at room temperature [11,12], although at an increasing temperature to 473-573 K, their performance decreased significantly [13,14]. However, due to CO and H_2SO_4 production during the adsorption and regeneration reactions [15,16], the use of these adsorbents at high temperatures and for high SO_2 concentrations is not as economically efficient for industrial operations as the Claus process.

Therefore, compared with other methods, the use of a dry regenerative solid sorbent is a more favored approach for the removal of SO_2. Over the last decades, researchers have investigated the SO_2 removal ability of various dry regenerative solid sorbents, such as metal oxides and silica-based mesoporous materials. For example, the characterization and removal capacity of different metal oxides, such as Zn, Mg, Ca, Al, Ti, Mn, Ce, and Cu oxides, have been studied [17-21]. Studies have found that the best absorbent of SO_2 is CuO and, accordingly, research has been conducted to improve its adsorption [22-25]. Centi et al. [26] investigated the mechanism for SO_2 oxidation-adsorption on CuO over alumina. Gavaskar et al. [27] developed and evaluated the ability of CuO adsorbents to remove SO_2 and also investigated the effect of temperature on the removal ability. Zhao et al. [28] studied the SO_2 removal capacity of NiAl mixed oxides. Lee et al. [29] used ZnO nanoparticles as sorbents for a low concentration of sulfur compounds. Lee et al. [30] also investigated the effect of Fe_2O_3 on the adsorption performance of CuO-Fe_2O_3 sorbents with a SiO_2 base.

The exhaust gases produced by a Claus unit include large quantities of H_2S and SO_2. The concentration of these acid gases was estimated to range from 5,000 to 30,000 ppm. For the proposed process, shown in Fig. 1, a two-column fixed bed of solid metal oxide adsorbents is used for the adsorbing process. The difference between this method and the method in which amine is applied is

†To whom correspondence should be addressed.
E-mail: ehsanimr@cc.iut.ac.ir

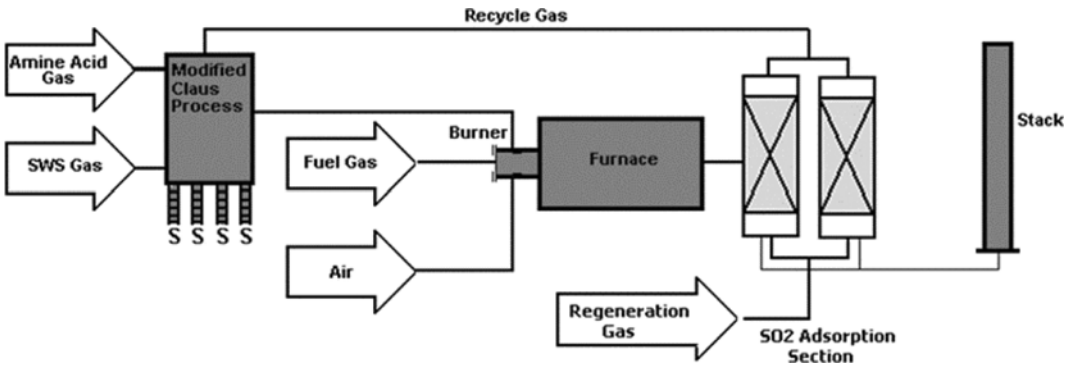

Fig. 1. Schematic diagram of proposed SO_2 adsorption process.

the adsorbed pollutant. For example, the amine absorption unit proceeds in the continuation of the Claus process, while the proposed adsorption unit converts H_2S to SO_2. This adsorption leads to a reduction in the amount of pollutants in the flue gas.

The advantages in using regenerative solid metal oxides to adsorb SO_2 have attracted the attention of Nano scientists. For this study, the effects of temperature and the initial concentration of SO_2 (10,000 to 30,000 ppm) on the process of SO_2 adsorption, should be studied using different concentrations of nanoscale metal oxides under various experimental temperatures.

EXPERIMENTAL APPROACH

1. Materials

Nano TiO_2 (TECNAN), without any purifications, was used as the adsorbent base. NaOH (Merck) was used to adjust the pH.

2. Adsorbent Preparation

To prepare the nano Fe_2O_3-CuO/TiO_2 adsorbent, a glass reactor was used in a silicone oil bath. The typical procedure for making the adsorbents is similar to the procedure used by Lee et al. [30]. A suitable amount of powder was dissolved in a mixture of $Cu(NO_3)_2$-$Fe(NO_3)_3$ to produce the required CuO and Fe_2O_3 percentages. Nano TiO_2 was gradually stirred into a mixture of $Cu(NO_3)_2$-$Fe(NO_3)_3$; the slurry was stirred for 2 h. The pH of the solution was adjusted to 8 during stirring by the dropwise addition of NaOH (0.5 M). The mixture was aged for 30 min, then filtered and washed with 500 ml deionized water. The wet cake that was produced was dried at 353 K for 12 h, and then calcined at 573 K for 4 h in a furnace.

3. Design of Experiments

To determine the effect of the experimental parameters on the SO_2 adsorption capacity of the adsorbents, as well as to reduce costs and experimental test time, the Taguchi design method was used. To investigate the optimum conditions for SO_2 adsorption capacity, the inlet concentration of SO_2, adsorption temperature, and adsorbent type were each considered at three levels (Table 1). Two L_9 orthogonal arrays were designed to compare the effect of the adsorbent arrangement, which is the wt% of the metal oxides, on adsorption performance.

Analysis of variance (ANOVA) was used to evaluate the results of each group and the effect of the parameters on the adsorption

Table 1. Experimental parameters and levels

Adsorbent		Temperature (K)	Concentration (ppm)
CuFeTi1 (n-CuO 10%, n-Fe_2O_3 15%)	CuFeTi2 (n-CuO 12%, n-Fe_2O_3 13%)	523	10000
CuFeTi3 (n-CuO 15%, n-Fe_2O_3 10%)	CuFeTi5 (n-CuO 20%, n-Fe_2O_3 5%)	573	20000
CuFeTi6 (n-CuO 22%, n-Fe_2O_3 3%)	CuFeTi4 (n-CuO 17%, n-Fe_2O_3 8%)	623	30000

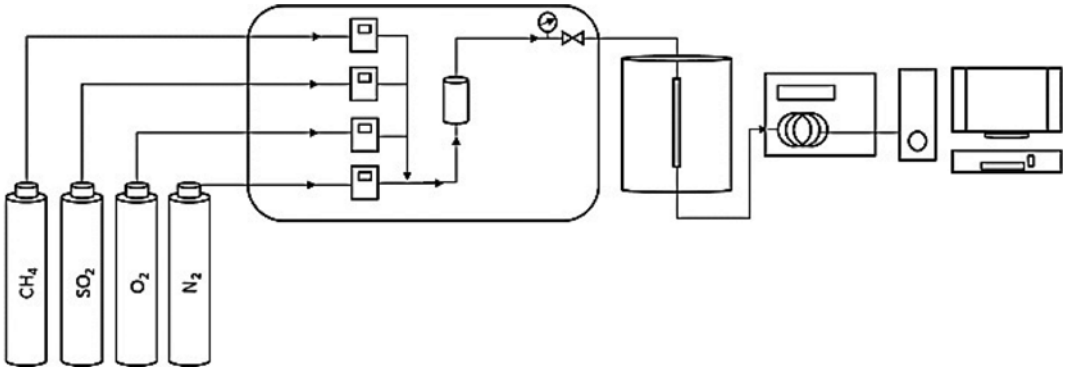

Fig. 2. Schematic diagram of laboratory adsorption setup.

Table 2. Orthogonal array of operational parameters

Experiment no.	Adsorbent		Temperature (K)	SO_2 concentration (ppm)
1, 2	CuFeTi1	CuFeTi2	523	10000
3, 4	CuFeTi1	CuFeTi2	573	20000
5, 6	CuFeTi1	CuFeTi2	623	30000
7, 8	CuFeTi3	CuFeTi5	523	20000
9, 10	CuFeTi3	CuFeTi5	573	30000
11, 12	CuFeTi3	CuFeTi5	623	10000
13, 14	CuFeTi6	CuFeTi4	523	30000
15, 16	CuFeTi6	CuFeTi4	573	10000
17, 18	CuFeTi6	CuFeTi4	623	20000

performance. The three available categories for ANOVA are smaller is better, nominal is better, and bigger is better [31].

4. Adsorption Analysis

The experimental adsorption tests were in a laboratory fixed bed reactor shown in Fig. 2. The fixed bed reactor contained a stainless steel cylindrical tube with a diameter of 12.7 mm and a length of 300 mm fixed vertically in a furnace. The bottom of the reactor was filled with a stainless steel net and glass wool to prevent any loss of powder by the gas stream. The sorbent (0.5 g, under mesh 80) was placed in the reactor with enough glass wool to prevent fluidization. During the adsorption tests, O_2 (5% v/v), SO_2 (Table 2), and N_2 gases were used as carrier gases to simulate the flue gas. The mass flow rate of each gas was controlled by a mass flow controller (MFC-Dwyer). The system path was purged with a neutral gas (N_2) for 30 min to avoid the presence of other gases during the adsorption process. Streams of N_2, O_2, and SO_2 accumulated in a small chamber, and an outlet valve was used to vent the gases for 15 min to obtain a uniform flue gas. The inlet valve of the reactor was opened and the output concentration of SO_2 was monitored continuously by gas chromatography (GC) with a flame photometric detector (FPD) until the SO_2 concentration reached an equilibrium state. The analyzed data from the GC were plotted for each test by computer as an adsorption isotherm.

5. Adsorption Mechanism

Metal oxide SO_2 adsorption mechanism was widely discussed by previous researchers [1,2]. Metal oxides generally react with SO_2 as follows:

$$M_xO_y + ySO_2 + \frac{y}{2}O_2 \rightarrow M_x(SO_4)_y \quad (1)$$

CuO, Fe_2O_3 and TiO_2 reaction with SO_2 proceed as follows:

$$CuO + SO_2 + \frac{1}{2}O_2 \rightarrow Cu(SO_4) \quad (2)$$

$$Fe_2O_3 + 3SO_2 + \frac{3}{2}O_2 \rightarrow Fe_2(SO_4)_3 \quad (3)$$

$$TiO_2 + 2SO_2 + O_2 \rightarrow Ti(SO_4)_2 \quad (4)$$

Research findings showed that CuO had a higher SO_2 adsorption among the single metal oxides [22-25,32]. The adsorbent temperature stability was improved by the use of Fe_2O_3 at moderate temperatures. However, the Fe_2O_3 adsorption capacity decreased as the temperature increased [33]. Since TiO_2 adsorbs SO_2 mostly by physisorption rather than chemisorption, Luo et al. [34] investigated the adsorption capacity of TiO_2 and found that maximum adsorption was at 393 K. They also found that as the temperature increased to 513 K, the adsorption capability reduced dramatically.

6. General Procedure of Experiments

Each category of adsorbents (as shown in Table 1) was first tested in nine experiments. To improve the accuracy of the tests, all the tests were repeated. If the deviation was greater than 5% for the results of each test, the experiment was repeated a third time to achieve more accurate calculations. All adsorption curves were presented as the mean of two of the accepted tests.

7. Characterization

The nano-adsorbent sample CuFeTi4 showing the best SO_2 removal performance in the experimental tests was analyzed with a field emission scanning electron microscope (FESEM), X-ray diffraction (XRD), and Brunauer-Emmett-Teller (BET) analysis. The FESEM images were collected using a Hitachi S4160 Cold Field Emission microscope at an accelerating voltage of 30 KV. The surface area and the pore size distribution of samples were calculated using BET and Barrett-Joyner-Hallenda (BJH) methods, respectively. Prior to the analyses, the samples were dried at 393 K for 15 h. XRD tests were carried out using an XPert MD model diffractometer at 30 mA and 40 kV.

The FESEM images of the CuFeTi4 adsorbent morphology are shown in Fig. 3. According to these images, the average size of the particles of CuFeTi4 was approximately 23-50 nm and their appear-

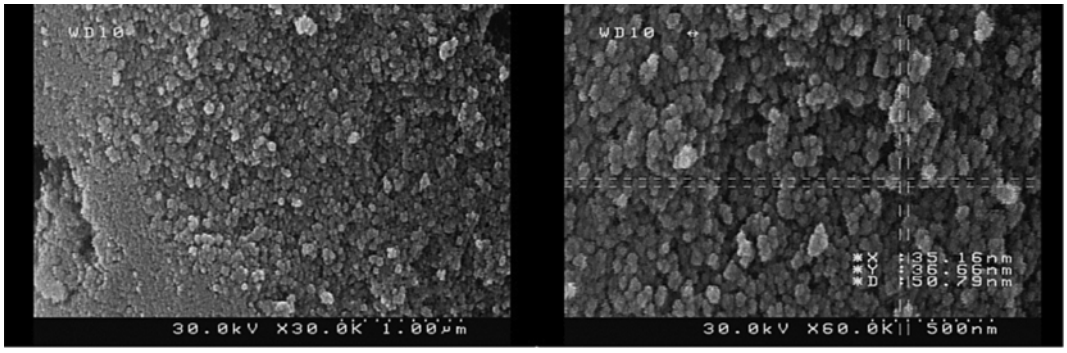

Fig. 3. SEM images of CuFeTi4 (17% n-CuO, 8% n-Fe_2O_3).

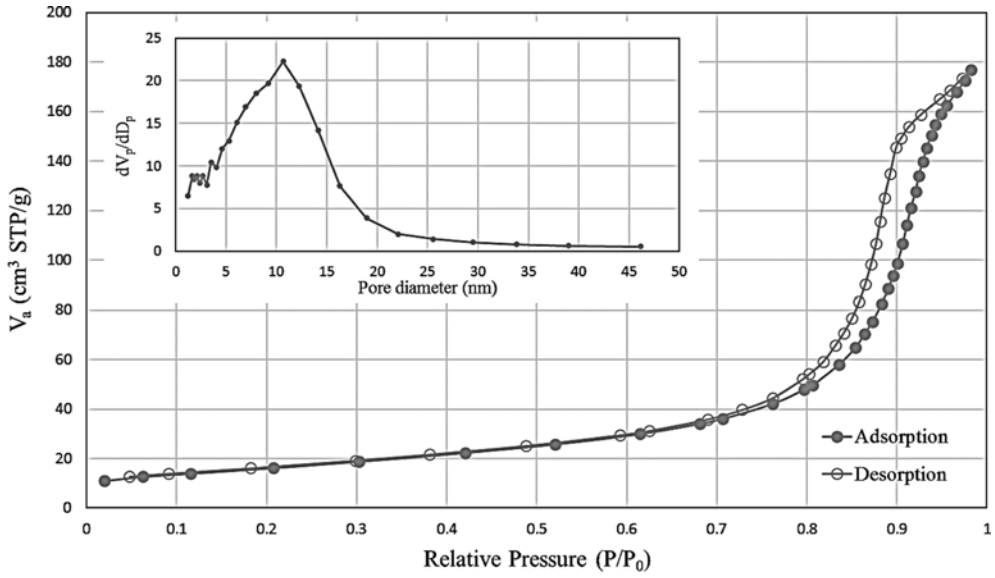

Fig. 4. Pore size distribution - N_2 adsorption/desorption analysis of CuFeTi4.

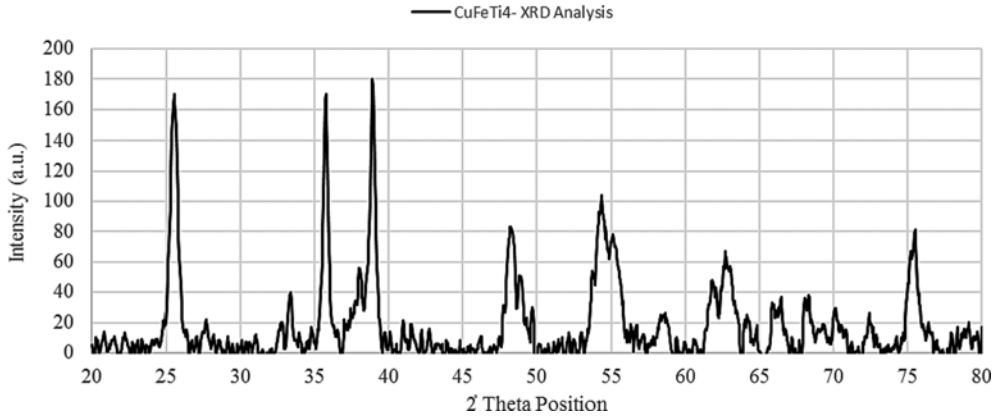

Fig. 5. CuFeTi4 (17% n-CuO, 8% n-Fe_2O_3) XRD pattern.

ance was uniform. The pore size distribution and the nitrogen adsorption-desorption profile of CuFeTi4 are shown in Fig. 4. The sample had a maximum pore size of approximately 10 nm. Furthermore, the nitrogen adsorption-desorption isotherm of CuFeTi4 can be classified as a type IV isotherm, which usually occurs for porous adsorbents with a pore size in the range of 1.5-100 nm. The specific surface area of CuFeTi4 according to the BET surface area analysis was nearly 73 m^2/g with a total pore volume of 0.27 cm^3/g.

XRD Pattern for CuFeTi4 showed 7 sharp peaks as illustrated in Fig. 5. Considering that, the peaks at 2θ=25.35, 38.96, 48.37 and 53.92 matched with TiO_2 anatase (00-004-0562), peaks at 2θ= 35.74, 38.96 and 54.58 matched with CuO tenorite (01-072-0629), also peaks at 2θ=35.74, 54.58, 62.26 and 75.37 matched with Fe_2O_3 hematite (00-003-0812).

RESULTS AND DISCUSSION

1. Adsorption Isotherms

Figs. 6-8 show the adsorption isotherms of each adsorbent for different SO_2 inlet concentrations and at different temperatures. In general, for all adsorbents, as the SO_2 inlet concentration increased, the initial output concentration increased; none of the adsorbents in a 0.5 g fixed-bed column could completely remove the SO_2 in the range of 10,000 to 30,000 ppm. Fig. 6 compares CuFeTi1 and CuFeTi2 at different conditions; as the temperature and SO_2 inlet concentration increased to 623 K and 30,000 ppm, respectively, the breakthrough time for both adsorbents decreased. However, at 623 K and 30,000 ppm, the adsorption performance of CuFeTi1 and CuFeTi2 became similar and the breakthrough time did not decrease as expected. The deactivation rates for both adsorbents increased as the temperature and concentration increased. Fig. 7 shows the performance of CuFeTi3 and CuFeTi5 under similar conditions. As expected, at higher temperatures and lower concentrations, 623 K and 10,000 ppm, respectively, CuFeTi3 and CuFeTi5 had the best adsorption performance, although the deactivation rate of these adsorbents was low and the adsorbents had to partially adsorb SO_2 for about 10 min to become saturated. A comparison of the adsorption of CuFeTi3 and CuFeTi5 showed that

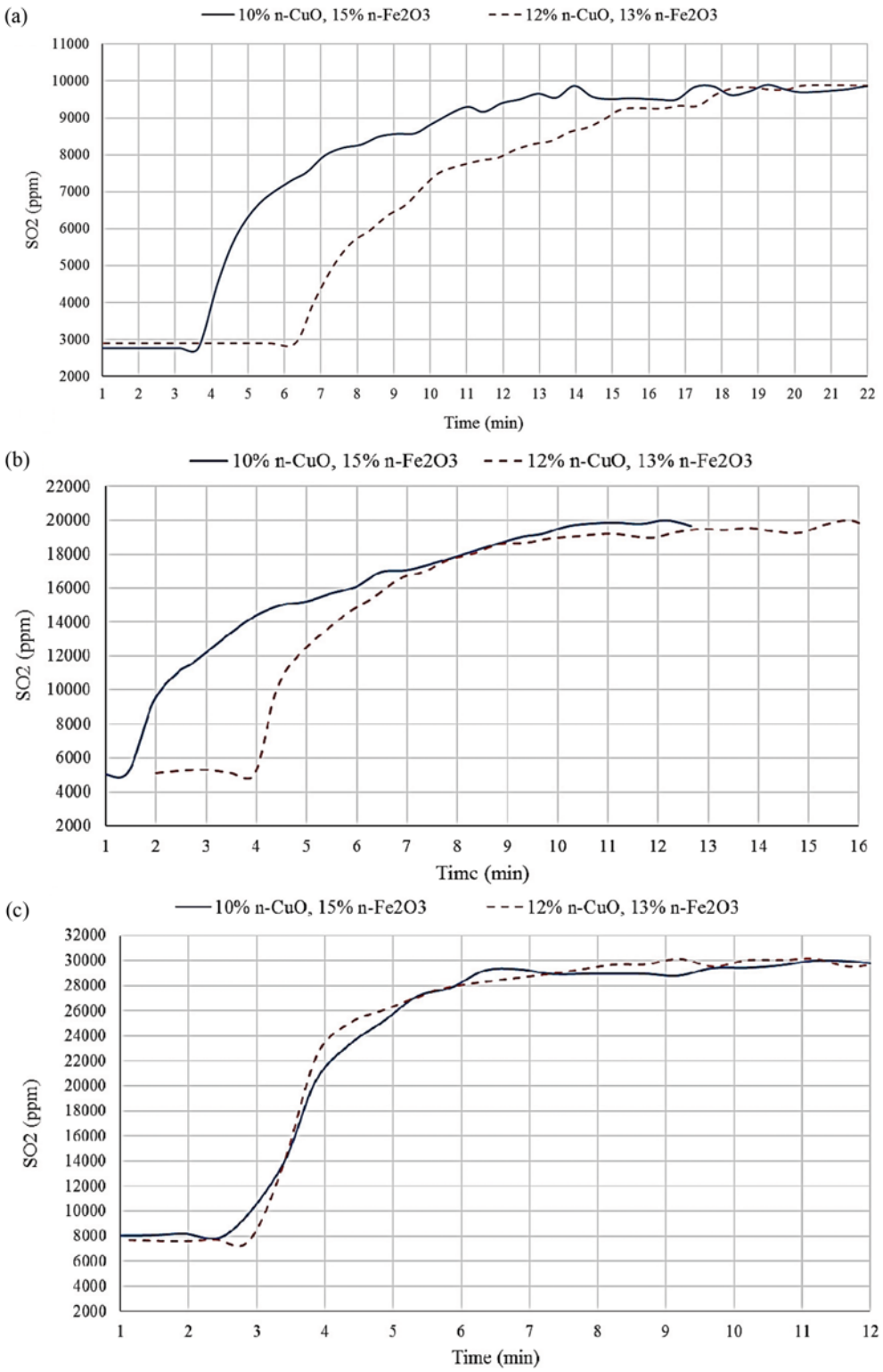

Fig. 6. Adsorption isotherm of CuFeTi1 and CuFeTi2 (a) 523 K - 10,000 ppm, (b) 573 K - 20,000 ppm, (c) 623 K - 30,000 ppm.

CuFeTi3 exhibited more SO_2 adsorption. The adsorption isotherms of CuFeTi4 and CuFeTi6 are shown in Fig. 8. CuFeTi4 had a more suitable performance CuFeTi6 in terms of breakthrough time and deactivation rate than CuFeTi6, except at a minimum temperature and maximum concentration, which were the worst conditions for adsorption. Considering all the isotherms in a variety of operational parameters, CuFeTi3 and CuFeTi4 showed the best SO_2 removal performance in terms of maximum breakthrough time, high deactivation rate, and initial SO_2 output concentration.

The adsorption curves in Figs. 6-8 show an increase in adsorp-

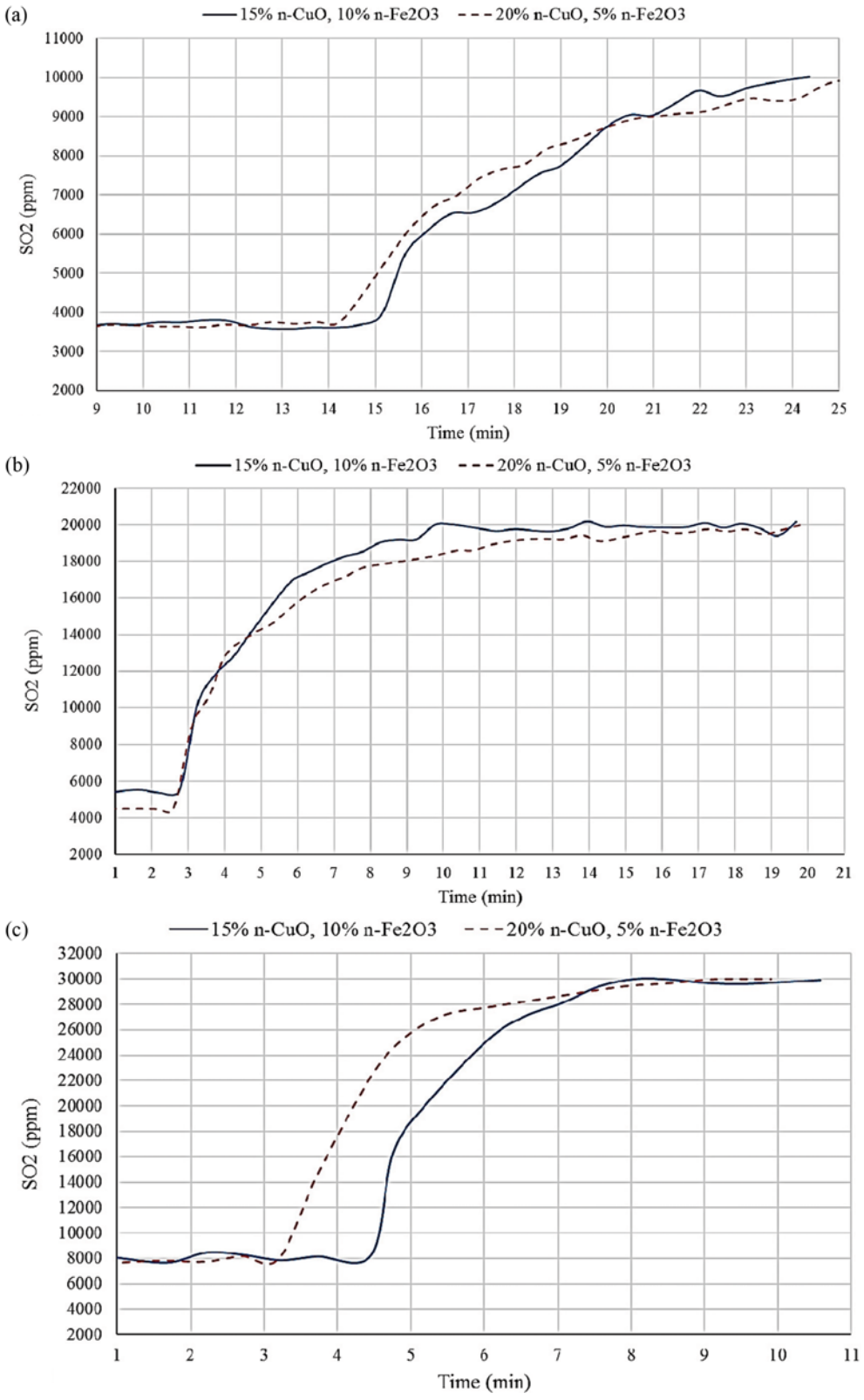

Fig. 7. Adsorption isotherm of CuFeTi3 and CuFeTi5 (a) 623 K - 10,000 ppm, (b) 523 K - 20,000 ppm, (c) 573 K - 30,000 ppm.

tion rate as the temperature increases from 523 K to 623 K. This confirms the results of Gavaskar et al. [27] for the adsorption of CuO-based adsorbents. Similarly, Ma et al. [15] studied Fe/activated coke and showed that increasing the temperature from 423 K to 523 K causes higher SO_2 adsorption. The increase in reaction rate occurred as a result of the endothermic reaction between the metal

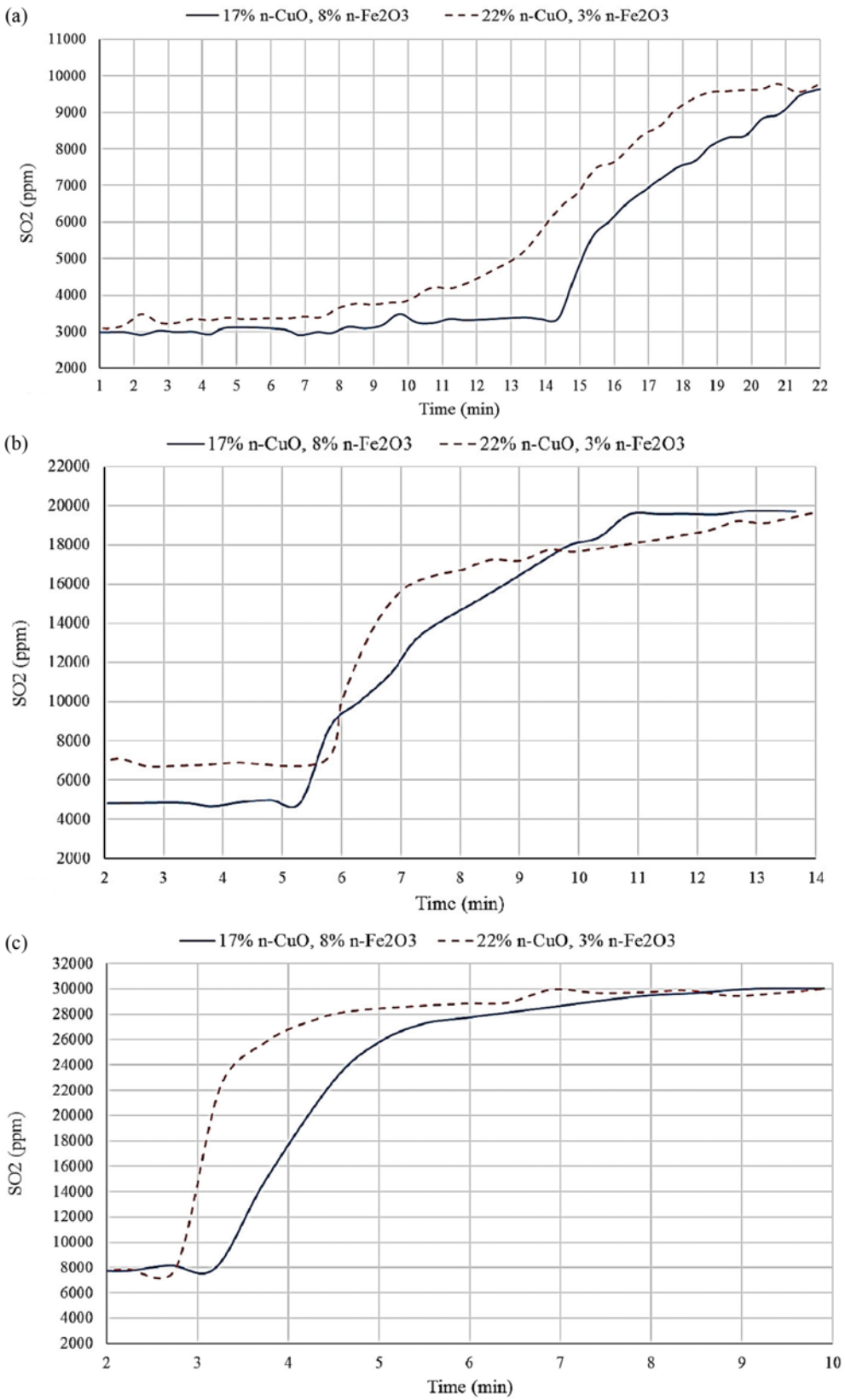

Fig. 8. Adsorption isotherm of CuFeTi4 and CuFeTi6 (a) 573 K - 10,000 ppm, (b) 623 K - 20,000 ppm, (c) 523 K - 30,000 ppm.

oxide and the SO_2 during adsorption. However, a further increase in temperature led to the sintering of the adsorbents.

Unlike temperature, increasing the SO_2 inlet concentration led to a decrease in adsorption rate due to pore plugging. In compari-

son, at low inlet SO_2 concentrations, the adsorbent bed became saturated earlier, while the SO_2 uptake happened faster at higher SO_2 concentrations. Luo et al. [34] reported the same effect of SO_2 concentration on the physical adsorption capacity of nano TiO_2.

The integration method was used to investigate the SO_2 adsorption capacity under experimental conditions. To evaluate the performance of the adsorbents, the amount of SO_2 that was adsorbed by the loaded adsorbents (0.5 gr) was calculated using Eq. (1).

$$SAC = \frac{Mw \times Q \times C_i}{\nu_m \times 10^6}\left(t_a - \int_0^{t_a} \frac{C}{C_i} dt\right) \quad (1)$$

where SAC represents SO_2 adsorption capacity (mg SO_2 per 0.5 gr sorbents); Mw is SO_2 molecular weight (~64 g/mol); Q is volumetric ratio (ml/min); C_i and C are initial and instant output SO_2 concentration (ppm); ν_m is molar volume of SO_2 at standard pressure and 298 K (24.45 lit/mol) and ta is fully saturation time (min). Calculated amounts of SACs are represented in Table 3.

For experiments 1 and 2, as shown in Table 3, 523 K and 10,000 ppm of SO_2 concentration, the SAC of CuFeTi1, which had 10% n-CuO and 15% n-Fe_2O_3, was 12.37 g SO_2/0.5 g sorbent. There was an increase in SAC for CuFeTi2, which had 12% n-CuO and 13% n-Fe_2O_3, at the same temperature and concentration of SO_2: 18.6337 g SO_2/0.5 g sorbent. This result is mainly because of the high SAC of CuO; an increase in CuO content leads to a higher capacity of the adsorbent. Additionally, low amounts of n-Fe_2O_3 guarantee the stability of the adsorbent. The increment of SAC with the addition of n-CuO content in samples continued until the SAC of CuFeTi4, which had a composition of 17% n-CuO and 8% n-Fe_2O_3; it reached 31.65 g SO_2/0.5 g sorbent, which is the highest SAC in all samples. However, from this point, any increase in CuO percentage led to a decrement in the SAC of the adsorbent due to agglomeration and the sintering of CuO particles (see experiments 13 and 14 in Table 3). Moreover, increasing the n-Fe_2O_3 content cannot compensate for the effect of CuO agglomeration and sintering since it has a scanty range of SAC. In similar studies, Gavaskar et al. [27] and Buelna et al. [10] investigated different CuO loading on γ-Al_2O_3 and showed that the optimum CuO loading was 14%.

2. The Analysis of Variance (ANOVA)

Using SACs as raw data and choosing the bigger is better mode, an ANOVA was performed for two separate groups of adsorbents; the results are given in Table 4 and Table 5. From the calculated parameters contribution for each group, it can be determined that temperature is the most prominent parameter for SO_2 adsorption with over 45% and 66% participation for group 1 and group 2,

Table 3. SO_2 adsorption capacity of sorbents

No.	Sorbent	Temp. (K)	SO_2 concentration (ppm)	SAC (g SO_2/0.5 g sorbent)	Removal percentage %
1	CuFeTi1	523	10000	12.37	72.44
2	CuFeTi2	523	10000	18.63	71
3	CuFeTi1	573	20000	16.23	74.45
4	CuFeTi2	573	20000	23.23	74.4
5	CuFeTi1	623	30000	22.87	74.31
6	CuFeTi2	623	30000	23.85	72.7
7	CuFeTi3	623	10000	31.56	63.56
8	CuFeTi5	623	10000	30.61	65
9	CuFeTi3	523	20000	17.45	73.5
10	CuFeTi5	523	20000	15.02	77.49
11	CuFeTi3	573	30000	27.92	74.2
12	CuFeTi5	573	30000	25.84	72.15
13	CuFeTi4	573	10000	31.65	70.2
14	CuFeTi6	573	10000	28.6	69.2
15	CuFeTi4	623	20000	29.02	74.76
16	CuFeTi6	623	20000	24.30	68.96
17	CuFeTi4	523	30000	21.05	75.26
18	CuFeTi6	523	30000	20.29	75.69

Table 4. ANOVA analysis of CuFeTi1, CuFeTi3 and CuFeTi6

Group 1: CuFeTi1, CuFeTi3 and CuFeTi6					
Factors	DOF	Sum of squares	Variance	Pure sum	Contribution %
Adsorbent	2	125.995	62.997	122.48	37.770
Temperature	2	151.936	75.968	148.421	45.770
SO_2 concentration	2	42.823	21.411	39.308	12.122
Other/error	2	3.514	1.757	-	4.338
Total	8	324.271		-	100

Table 5. ANOVA analysis of CuFeTi2, CuFeTi5 and CuFeTi4

Group 2: CuFeTi2, CuFeTi5 and CuFeTi4					
Factors	DOF	Sum of squares	Variance	Pure sum	Contribution %
Adsorbent	2	43.84	21.92	40.52	16.295
Temperature	2	168.105	84.052	164.785	66.269
SO_2 concentration	2	33.396	16.698	30.077	12.095
Other/error	2	3.318	1.659	-	5.341
Total	8	248.661	-	-	100

respectively. Moreover, when the parameter contributions for group 1 and group 2 were compared, it appeared that changing the accretion order of CuO percentage and decreasing the order of Fe_2O_3 percentage in the adsorbents by varying the arrangement, the inlet concentration contribution of SO_2 was independent of the effect of interaction and remained in a constant range. However, the temperature and adsorbent percentage were changed in the SO_2 adsorption.

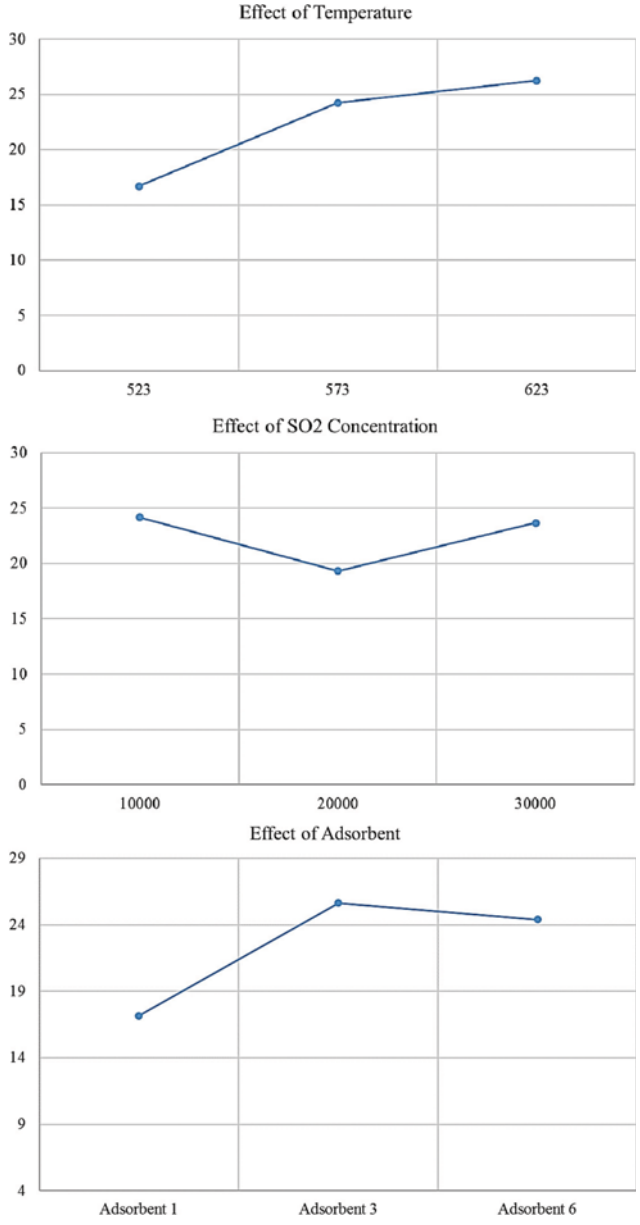

Fig. 9. Group 1 SAC mean effect of levels.

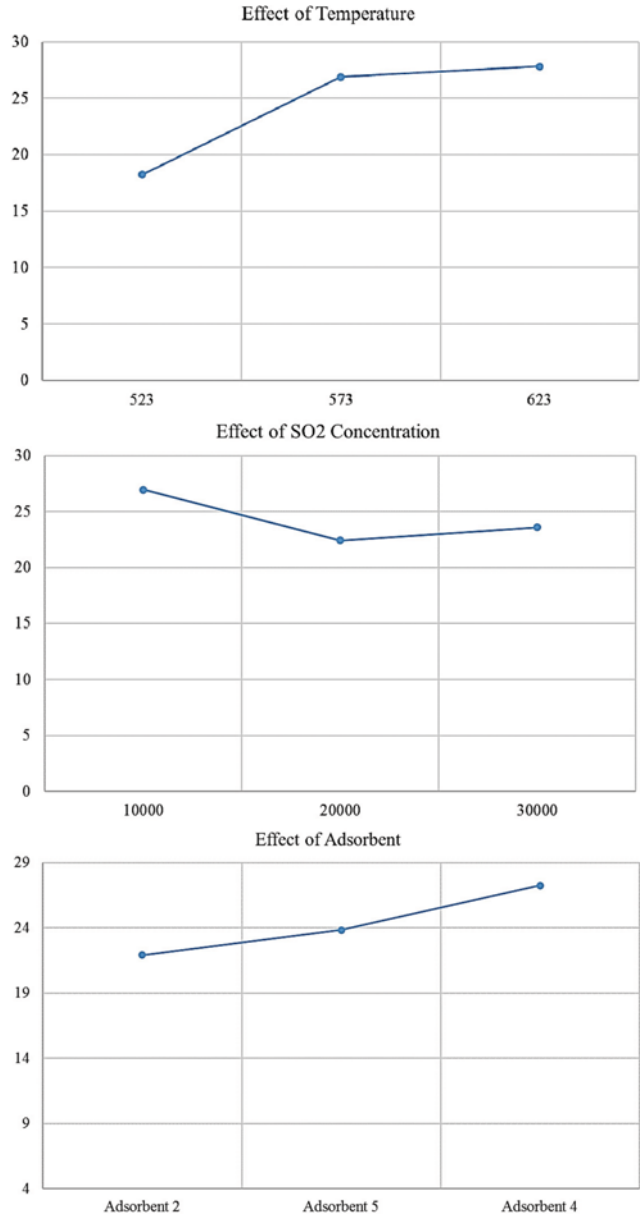

Fig. 10. Group 2 SAC mean effect of levels.

The mean amount of SO_2 adsorption capacity for each experimental parameter can be calculated by using Eq. (2).

$$\overline{A}_L = \frac{\sum_{@L,\, i=1}^{n} SAC_i}{N} \quad (2)$$

where $\overline{A}_L$, defines mean effect of parameter A in the level L, N is the number of levels.

The mean effect for all levels of experimental parameters was calculated (Fig. 9 and Fig. 10). The optimum levels showed the higher SAC. Based on Fig. 10, 623 K and 10,000 ppm and CuFeTi3 are the optimum levels for the best result of adsorption. Similarly, as can be seen in Fig. 10, 623 K and 10,000 ppm and CuFeTi4 are the optimum conditions. The SAC of the adsorbents increased when the temperature increased to 623 K, although higher temperatures led to agglomeration or degradation of adsorbent, which caused significantly lower SAC. CuFeTi3 and CuFeTi4 were the most capable adsorbents in the desulfurization process at a ratio of 31.56 mg SO_2/0.5 g sorbent (at 10,000 ppm, 623 K) and 31.65 mg SO_2/0.5 g sorbent (at 10,000 ppm, 573 K), respectively. As shown by the mean effect of levels on SAC, it is expected that for CuFeTi4, increasing the temperature to 623 K, increased the SAC to 33.384 mg SO_2/0.5 g sorbent. An experimental adsorption test for CuFeTi4 at optimum conditions (10,000 ppm, 623 K) exhibited 32.71 mg SO_2/0.5 g sorbent desulfurization with a 2% deviation, which is an acceptable experimental error.

By increasing the SO_2 concentration, it is expected that due to the higher mass transfer rate, there is an increase in the reaction rate and the removal percentage; this can be seen in Table 3. Fig. 9 and Fig. 10 show the mean gained results for the adsorbents. Considering that 30,000 ppm was used for the experimental conditions, these figures and Table 4 and Table 5 show that, because of the greater effect of temperature compared with inlet concentration, an inlet concentration between 10,000 and 30,000 ppm higher average results, caused due to extensively more temperature effect toward inlet concentration on adsorption amount.

With regard to the performance of the adsorbents and the percentage amount of metal oxides, the results showed that a combination of 17% CuO and 8% Fe_2O_3 was more suitable for SO_2 removal.

CONCLUSION

CuO is one of the best SO_2 adsorbents. According to the obtained experimental results, the adsorption rate of Fe_2O_3 was lower than that of CuO. However, it was used because of its catalytic activity for the conversion of SO_2 to SO_3, which leads to better adsorption and provides good recovery properties to the adsorbent.

The effect of temperature and concentration of SO_2 was evaluated according to the adsorption performance of the adsorbents. The temperature had the largest impact on the adsorption rate of the adsorption bed. The type of adsorbent and the concentration of SO_2 also had an impact on the adsorption. In this research, the type of adsorbent was represented as the different percentages of metal oxides.

The results for the first group of adsorbents showed that the adsorbent with a composition of 15% CuO and 10% Fe_2O_3 particles had the highest adsorption at 623 K and in a concentration of 10,000 ppm. The maximum adsorption for CuFeTi3 was about 31.5 mg SO_2/0.5 g adsorbent. Due to the adsorption bed onset saturation time, the adsorbent containing 15% CuO and 10% Fe_2O_3 had the best performance compared with the other adsorbents. However, another important parameter that determined the most suitable adsorbent was the optimal time in which the adsorbent was used.

In the second group of adsorbents, the adsorbent containing 17% CuO and 8% Fe_2O_3 had the highest SO_2 adsorption among all the adsorbents. The maximum adsorption at 623 K for a concentration of 10,000 ppm was about 32.5 mg SO_2/0.5 g adsorbent.

The BET analysis of CuFeTi3, which contained 15% CuO and 10% Fe_2O_3, showed that it had a surface area of 72 m^2/g; this was the same as CuFeTi4, which contained 17% CuO and 8% Fe_2O_3. However, CuFeTi4 had the highest adsorption, while CuFeTi3 adsorbed less SO_2. The only difference between the two adsorbents was their percentage of metal oxides. Therefore, high levels of CuO (up to 17% by mass) and a low percentage of Fe_2O_3 (about 8% by mass) have an effective impact on the adsorption of SO_2.

Temperature had a direct effect on the adsorption of SO_2 in the experimentally tested range. As the temperature increased, it caused damage to the adsorbents due to degradation and agglomeration, which reduced the available specific surface area. Consequently, the rate of mass transfer decreased, which lowered the adsorption capacity of the adsorbents.

To use this method on a semi-industrial scale, investigations should be performed into the surface modification of the adsorbents using a support with a more surface area, granulation to control the agglomeration caused by powder or the transfer of powder by gas flow, and the strength of the adsorbents, durability, and cycling effects.

NOMENCLATURE

v_m : molar volume of SO_2 at standard pressure and 298 K [Lit/mol]
$\overline{A}_L$: mean effect of parameter A in the level L
C : ppm
C_i : ppm
MW : molecular weight [g/mol]
N : number of levels
Q : volumetric ratio [ml/min]
SAC : SO_2 adsorption capacity [mg SO_2/0.5 gr sorbents]
t_a : fully saturation time [min]

REFERENCES

1. R. Bahrami, H. Ale Ebrahim and R. Halladj, *Process Saf. Environ. Prot.*, **92**, 938 (2014).
2. Y. Mathieu, M. Soulard, J. Patarin and M. Moliere, *Fuel Process. Technol.*, **99**, 35 (2012).
3. E. Atanes, A. Nieto-Márquez, A. Cambra, M. C. Ruiz-Pérez and F. Fernández-Martínez, *Chem. Eng. J.*, **211**, 60 (2012).
4. S. J. Lee, S. C. Lee, S. Y. Jung, C. K. Ryu and J. C. Kim, *Korean J.*

Chem. Eng., **26**, 1286 (2009).
5. L. Zhao, X. Li, C. Hao and C. L. Raston, *Appl. Catal., B*, **117-118**, 339 (2012).
6. W. N. W. Abdullah, W. A. W. A. Bakar and R. Ali, *Korean J. Chem. Eng.*, **32**, 1999 (2015).
7. J. A. Lagas, J. Borsboom and P. H. Berben, *Oil Gas J.*, **86:41**, 66 (1988).
8. M. P. Elsner, M. Menge, C. Muller and D. W. Agar, *Catal. Today*, **79-80**, 487 (2003).
9. D. Jones, D. Bhattacharyya, R. Turton and S. E. Zitney, *Ind. Eng. Chem. Res.*, **51**, 2362 (2011).
10. G. Buelna and Y. Lin, *Sep. Purif. Technol.*, **39**, 167 (2004).
11. Y. Mathieu, L. Tzanis, M. Soulard, J. Patarin, M. Vierling and M. Moliere, *Fuel Process. Technol.*, **114**, 81 (2013).
12. H. P. Ho, P. Kasinathan, J. Kim, D. Lee and H. C. Woo, *Korean J. Chem. Eng.*, **33**, 1908 (2016).
13. M. A. Alvarez-Merino, F. Carrasco-Marin and C. Moreno-Castilla, *Appl. Catal., B, Environ.*, **13**, 229 (1997).
14. J. Guo and A. C. Lua, *J. Chem. Technol. Biotechnol.*, **75**, 971 (2000).
15. J. Ma, Z. Liu, S. Liu and Z. Zhu, *Appl. Catal., B, Environ.*, **45**, 301 (2003).
16. H. H. Tseng, M. Y. Wey, Y. Sh. Liang and K. H. Chen, *Carbon*, **41**, 1079 (2003).
17. S. Kikuyama, A. Miura, R. Kikuchi, T. Takeguchi and K. Eguchi, *Appl. Catal., A*, **259**, 191 (2004).
18. S. J. Lee, S. Y. Jung, S. C. Lee, H. K. Jun, C. K. Ryu and J. C. Kim, *Ind. Eng. Chem. Res.*, **48**, 2691 (2009).
19. L. S. Jae, H. K. Jun, S. Y. Jung, T. J. Lee, C. K. Ryu and J. C. Kim, *Ind. Eng. Chem. Res.*, **44**, 9973 (2005).
20. P. S. Lowell, K. Schwitzgebel, T. B. Parsons and K. J. Sladek, *Ind. Eng. Chem. Process Des. Dev.*, **10**, 384 (1971).
21. E. Schreier, R. Eckelt, M. Richter and R. fricke, *Appl. Catal., B*, **65**, 249 (2006).
22. S. M. Jeong and S. D. Kim, *Ind. Eng. Chem. Res.*, **36**, 5425 (1997).
23. C. Macken, B. K. Hodnett and G. Paparatto, *Ind. Eng. Chem. Res.*, **39**, 3868 (2000).
24. Z. H. Jia, Z. Y. Liu and Y. H. Zhao, *Chem. Eng. Technol.*, **30**, 1221 (2007).
25. J. Xiang, Q. Zhao, S. Hu, L. Sun, S. Su, P. Fu, A. Zhang, J. Qiu, H. Chen and M. Xu, *Asia Pac. J. Chem. Eng.*, **2**, 182 (2007).
26. G. Centi, N. Passarini, S. Perathoner and A. Riva, *Ind. Eng. Chem. Res.*, **31**, 1947 (1992).
27. V. S. Gavaskar and J. Abbasian, *Ind. Eng. Chem. Res.*, **45**, 5859 (2006).
28. L. Zhao, X. Li, Z. Qu, Q. Zhao, S. Liu and X. Hu, *Sep. Purif. Technol.*, **80**, 345 (2011).
29. Y. J. Lee, N. K. Park, G. B. Han, S. O. Ryu, T. J. Lee and C. H. Chang, *Curr. Appl. Phys.*, **8**, 746 (2008).
30. H. S. Lee, M. P. Kang, Y. S. Song, T. J. Lee and Y. W. Rhee, *Korean J. Chem. Eng.*, **18**, 635 (2001).
31. K. Li, Y. Wang, S. Wang, B. Zhu, S. Zhang, W. Huang and S. Wu, *J. Nat. Gas Chem.*, **18**, 449 (2009).
32. A. Biabani, M. Rezaei and Z. Fattah, *J. Nat. Gas Chem.*, **21**, 415 (2012).
33. M. D. Dolan, A. Y. Ilyushechkin, K. G. Mclennan and S. D. Sharma, *Asia Pac. J. Chem. Eng.*, **7**, 1 (2012).
34. Y. Luo and D. Li, *Dev. Chem. Eng. Mineral Process.*, **10**(3/4), 443 (2002).